A 1 × 8 Linear Ultra-Wideband Phased Array With Connected Dipoles and Hyperbolic Microstrip Baluns

RUOYU HE[1,2], **HONGBO ZHANG**[1,2], **CHAN HWANG SEE**[3,4], **(Senior Member, IEEE)**,
YAN SU[1,2], **YUE MA**[2,5], **DEQING KONG**[1,2], **XINYING ZHU**[1,2],
AND RAED ABD-ALHAMEED[3], **(Senior Member, IEEE)**

[1]Key Laboratory of Lunar and Deep Space Exploration, National Astronomical Observatories, Chinese Academy of Sciences, Beijing 100101, China
[2]School of Astronomy and Space Science, University of Chinese Academy of Sciences, Beijing 100049, China
[3]Faculty of Engineering and Information, University of Bradford, Bradford BD71DP, U.K.
[4]School of Engineering, University of Bolton, Bolton BL35AB, U.K.
[5]Joint Laboratory for Radio Astronomy Technology, National Astronomical Observatories, Chinese Academy of Sciences, Beijing 100101, China

Corresponding author: Ruoyu He (hery@nao.cas.cn)

ABSTRACT A 1×8 linear single polarized ultra-wideband connected dipole phased array with wide angle scan range is proposed. The dipoles in the array are connected with each other in E-plane to improve the impedance matching on the low end of the frequency band. The frequency band and the scan range in E-plane is 2∼9 GHz for broadside radiation, 2∼8 GHz for 30° scan, 2∼7 GHz for 45° scan, and 2∼6.5 GHz for 60° scan. The VSWR is better than 2.0 across the frequency band from 2 to 9 GHz for broadside radiation and the cross-polarization level is below −10 dB. A hyperbolic microstrip balun is used as an impedance transformer to connect the 50 Ω SMA connector to a 150 Ω broadband dipole in an array. The structure of this antenna is totally planar and low profile, thus it is made easy to integrate with the PCB boards. To eliminate the surface wave blindness, no other dielectric layer is used in the array. The proposed balun supports common mode (CM) current and the radiation of this CM current cancels the radiation of the dipole in some frequency for a certain scan angle, this results in feed blindness. Adding H-plane PEC walls decreases the feed blindness frequency in the design.

I. INTRODUCTION

Ultra-wide band phased array antennas with the properties of wide-angle scanning volume, low cross polarization and low profile are required increasingly by the ultra-wideband phased array radar systems and communication systems recently [1], [2]. The multifunctional aperture could cover many frequency bands and could be used as the antenna of both radar and communication systems [3]. Phased arrays with the property of steerable main beam, ultra-wide band, and wide scan volume are the good antenna for this aperture. The ultra-wide band is needed to improve the resolution of the radar system and the wide angle scanning volume helps to reduce the total number of antenna arrays needed in a phased array radar system for 360° scan. One good choice of antenna that met the requirement above is the Vivaldi array [4]. However, the Vivaldi array element is not a pla-

nar structure; rather a 3-dimensional structure which has a relatively high profile. In the wideband application case, for example, 4:1 bandwidth or wider, the height of the Vivaldi element is about 4 times of the element spacing [5], [6]. When scanned in the D-Plane, this high profile leads to high level of cross polarization [21], [32]. Moreover, the large height of the Vivaldi array element permits the presence of a vertical current component on the element itself. These vertical currents produce higher propagation modes which cause impedance mismatch when the scan angle is large, thus narrowing the bandwidth [7]. To combat this problem, the bunny ear combline Vivaldi antenna elements carved rectangular slots on the element itself to mitigate the vertical current component, and the higher propagation modes were eliminated with the operating bandwidth of 0.3∼1 GHz and ±45° scan volume [8]. However, this non-planar and tall

structure of the Vivaldi elements increase the manufacture difficulties, leading to a high producing cost, especially when dielectric loading is needed to achieve wider scan volume.

In the effort to reduce the profile, the array of electrically small, tightly coupled printed dipoles was discovered with the property of ultra-wideband, and a number of this kind of UWB arrays were proposed. Munk [9], [10] at Ohio State University studied this kind of antennas and introduced an equivalent circuit model to interpret and guide the design of such antennas. Munk *et al.* [11] also designed an ultra-wideband antenna array with large scan volume. Mark Jones and James Rawnick at Harris Corporation used the same circuit model theory and designed a phased array with bandwidth 9:1 (2-18 GHz) and scan the volume ±45° from broadside using tightly coupled dipoles [12]. Holland *et al.* [13] in University of Massachusetts at Amherst devised a 7~21GHz dual-polarized planar ultra-wideband modular array, while Doane *et al.* [14] in Ohio State University introduced an even more precise circuit model and incorporated an integrated balun to enhance the bandwidth to 7.35:1 with ±45° scanning volume. Later, William F. Moulder el al. proposed a tightly coupled dipole array with resistive Frequent Selective Surface (FSS) located halfway between the radiation aperture plane and the ground plane and obtain a 21:1 bandwidth [2]. These ultra-wideband antenna arrays showed that the ultra-wide band array could be composed of array elements that have a relative limiting bandwidth isolated, for example, the planar dipoles. However, these antenna arrays all need one or two dielectric layers put in front of array elements in order to further expand the frequency bandwidth, which was called the Wide Angthe the le Impedance Matching (WAIM) layers or dielectric loading [15]. However, the WAIM layers in front of the array could support surface waves in the dielectric layers, which result in scan blindness in the scan volume and impedance mismatch on the bandwidth. To overcome this issue, Holland and Vouvakis [16] suggested to drill holes in the WAIM layers to push the Feed Blindness out of the scan volume. In addition, the bulky dielectric layer in front of the array could increase the weight of the whole antenna considerably and could introduce loss to the antenna gain [17].

Moreover, J. J. Lee and S. Livingston studied the planar slot array, the counterpart of the planar dipoles, and devised the UHF long slot aperture antenna with a 4:1 bandwidth without the front dielectric layers, proving that the long slot array antenna could also achieve wide bandwidth [18], [19]. To further broaden the bandwidth, Lee *et al.* [20] proposed an ultra-wideband phased array using long slot arrays, which demonstrated a bandwidth of 10:1 (200-2000 MHz). But the feeding structure of the slot array is complex and may introduce common mode resonance on the vertical feed lines on certain scan angles [21]. The common mode resonance resulted from the mutual coupling between the unbalanced current on the vertical feed lines and the unbalanced current on array elements, causing total reflection on some scan angles [22].

In this paper, a 1×8 linear phased array with Connected Dipoles was presented. A Hyperbolic Microstrip Balun connected the Connected Dipoles to an SMA connector. The proposed antenna showed that the Connected Dipole configuration decreases the VSWR in the low end of the frequency band, resulting in a wider bandwidth, i.e. 2 GHz. The frequency limit on the high end of the band is determined by the grating lobes. The Connected Dipole array exhibits an operating band of 2~9GHz for broadside radiation, 2~8 GHz for E-plane 30° scan, 2~7GHz for E-plane 45° scan, and 2~6GHz for E-plane 60° scan. To verify the simulated result, a prototype was constructed with the Connected Dipole and microstrip balun was printed on a 1mm thickness PCB board. No other dielectric layer was used, thus, no surface wave blindness was observed in the scan range in the frequency band. Measured results showed that the VSWR is <2.0 on 1.8~11.8GHz for broadside radiation. The sidelobe levels are <−10dB on 2~9GHz for broadside radiation. The remainder of the paper is organized as follows. Section II gives the structure, sizes of the Connected Dipoles and the Hyperbolic Microstrip Balun. Section III describes the theory and design process of the proposed antenna by compromising the impedance mismatching on the low end of the frequency band and the onset of grating lobes on the high end. The VSWR of the Connected Dipole array and two traditional inter-digital dipole arrays with the same size are compared. The onset frequencies of the grating lobe of the point source array with the same element spacing are also shown. Section IV illustrates the simulated gain pattern of a 1×8 linear array for 0°, 30°, 45° and 60° scan in the E-plane. Section V discusses the measured results of a 1×8 linear array and the comparison between the simulated results and measured results. Section VI shows the infinite planar (2D) array design with the same dipoles as in the linear array. The phenomenon of E-Plane feed induced blindness is demonstrated and its forming theory is presented. This theory clarifies why the feed blindness happens only in E-Plane scan, not in H-Plane scan. It also points out that the feed blindness frequency is not equal for positive and negative scan angles. This is proven by using HFSS simulator. Two ways of changing the feed blindness frequency are also given in this section. Section VII presents a design of an infinite single polarized planar (2D) Connected Dipole array with ±60° scan volume in E-, H-, and D-Plane on 3~6GHz without feed blindness by introducing H-Plane PEC walls. Finally, the paper concludes in Section VIII and a comparison between the proposed planar array and other typical wide-angle wideband phased arrays is also shown here.

II. STRUCTURE AND SIZES OF CONNECTED DIPOLE ARRAY AND HYPERBOLIC MICROSTRIP BALUN

The overall proposed 1×8 phase linear array antenna is shown in Fig.1(a). As can be seen, it consists of a series of printed planar connected dipoles, baluns and a slotted metal plate. Both of the antenna array elements and baluns are printed on a substrate.
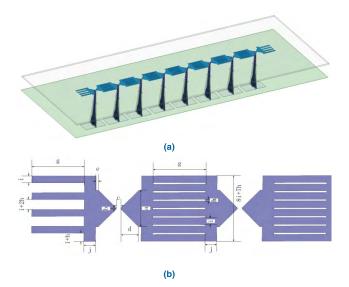
(a)

(b)

FIGURE 1. (a) Overall geometry of the proposed antenna phase array, (b) the planar connected dipole element.

TABLE 1. Geometric parameters of connected dipoles.

a	b	c	d
7mm	0.2mm	0.9mm	3.4mm
e	**g**	**h**	**i**
0.5mm	10mm	0.3mm	1.3mm
j	**Space**	**Width**	**s**
2.2mm	2×(**d**+**e**+**j**)+**g**+**c**=23.1mm	8×**i**+7×**h**=12.5mm	3.01mm
t	**u**	**v**	**w**
12.9mm	14mm	0.18	0.18
bb	**cc**	**k**	**l**
0.6mm	9.8mm	0.74mm	35mm

FIGURE 2. Dipole sheet of the 1×8 Linear Phased Array.

Dipoles are printed on a dielectric sheet of thickness 1mm and of material Taconic TLY 2.2as shown in Fig. 2. It should be noted that the two edge elements are different from the central elements.

FIGURE 3. The structure and dimensions of the hyperbolic microstrip balun. The exponent of the top hyperbola is 'v', and the exponent of the ground hyperbola is 'w'. All the parameter values are available in Table 1.

A. THE STRUCTURE OF CONNECTED DIPOLE

The proposed linear array consists of planar connected dipoles placed one after another in a row as illustrated in Fig. 1(b). The fundamental elements constituting this linear array are planar dipoles. The arms of a dipole in the row are connected with the arms of its adjacent dipole and the corresponding geometric parameters of the planar dipole are given in Table 1. As can be seen, seven slots with the length 'g' and width 'h' are carved on the planar dipole cell. The inter-element spacing of the planar dipoles in E-Plane is denoted as parameter 'space' in Fig. 1(b) and Table 1, which is 23.1mm long and equivalent to $0.15\lambda_{low}$ where λ_{low} is the wavelength at 2GHz. The 'width' of the planar dipole is equal to '8×i + 7 × h'. The feed point between two arms in a planar dipole is denoted as parameters 'b' and 'c', and from here a hyperbolic microstrip balun is introduced to connect the planar dipole and an SMA Connector. These Connected
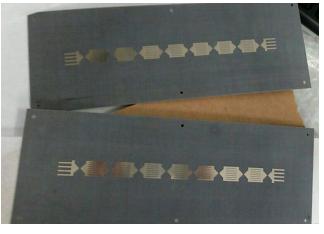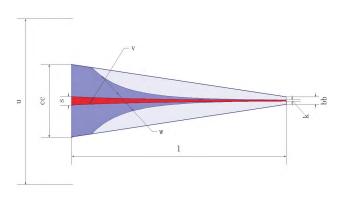
B. STRUCTURE OF HYPERBOLIC MICROSTRIP BALUN

The Connected Dipoles are fed differentially by implementing a hyperbolic microstrip balun. An SMA Connector is mounted on the left side of the Balun, and the planar dipole is connected to the right side of it as shown in Fig. 3. Both balun strips are printed on two sides of a 1 mm thickness dielectric sheet, which was also made of Taconic TLY 2.2 and has the shape of a trapezoid. The height of the balun is 'l' which is 35mm. The left end of the top strip 'v' is denoted as line 's', which is connected to the inner conductor of the Coaxial cable. The left end of the ground strip 'w' is denoted as line 'u', which is connected to the outer conductor of the Coaxial cable. However, the two angles of the metallic ground strip 'w' on the left end are cut off to fit in size on the trapezoid dielectric sheet. Notably, this cutting does not affect the performances of this balun. The prototype of
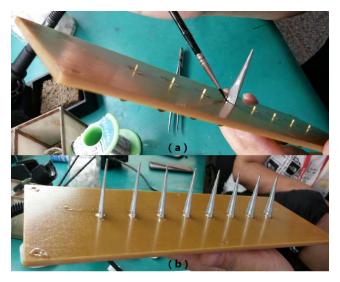
FIGURE 4. The Hyperbolic Microstrip Balun on a dielectric sheet. (a) The Ground strip in a Balun. (b) The top strip in a Balun. Note there are 8 Baluns on the dielectric sheet altogether.

FIGURE 5. Dipole arrays and their equivalent circuits. (a) Linear inter-digital dipole array. (b) The equivalent circuit for the inter-digital dipole array. (c) The Connected Dipole Array. (d) The equivalent circuit for the Connected Dipole Array.

this hyperbolic microstrip balun is fabricated and presented in Fig. 4.

III. THEORY AND DESIGN PROCESS

The antenna array consisting of electrically small, tightly coupled dipoles has shown the ultra-wideband property and wide-angle scanning in previous publications [9]–[14], and the structure of such antenna array can be described as in Fig. 5(a). The gap between adjacent dipole arms form a capacitor and the two arms of the dipole form two inductors as shown in the equivalent circuit of such array as illustrated in Fig. 5(b). The capacitor and the inductor are connected in series, which cause the reactance of the antenna moves above and below the middle frequency of the operating frequency band [24]. However, when introducing the ground to the structure, this reactance behaves in the opposite way. When the two reactance are shunt together, they cancel each other at the low end and high end of the frequency band, thus lead to a constant impedance of the dipole on the frequency band of about 4:1. Further, dielectric layers could be put on the dipole array for the wider bandwidth of about 5:1 [9]. However, the implementation of the above theory is limited by the low end of the frequency band. The impedance is difficult to remain constant in the lower end of the frequency band and results in an increase in VSWR, when the wavelength becomes increasingly large. A method of improving the impedance matching of the array on the lower frequency band is proposed here by connecting the adjacent dipole arms together, as shown in Fig. 5(c). The equivalent circuit of the Connected Dipole Array is given in Fig. 5(d).

By Examining the above two equivalent circuits as in Fig.5 (b,d), it is found that the equivalent capacitors between dipole arms not only rely heavily on between adjacent dipoles but also depend on the coupling between the two arms within one dipole as shown in Fig. 5(c-d). Thus,
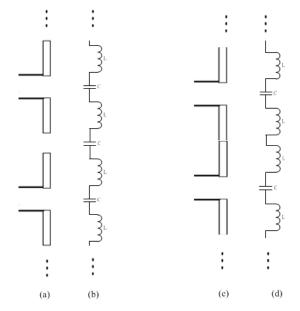
the arms of adjacent dipoles could be connected together. As can be noticed in Fig.5(d), it is the same as Fig.5 (b) except the capacitor in the middle of the structure is removed. Due to this reason, this proposed connected dipoles configuration could still cancel the impedance caused by the ground plane on the lower and higher end of the frequency band.

A. COMPARISON BETWEEN IMPEDANCE VARIATION OF CONNECTED DIPOLE ARRAY AND TWO SAME SIZE INTER-DIGITAL DIPOLE ARRAYS

To verify the above design concepts, three simulated models, i.e. Connected Dipole Array, two same size inter-digital dipole arrays, were designed by using Ansoft HFSS and CST. For better comparison, a 1×8 linear array was proposed for each model. Fig.6 shows the two traditional arrays are the same model as the connected arms configuration, but the arms of the planar dipoles are separated from the arms of its neighboring dipoles. Thus, the dipoles in the two traditional configurations have four digits at the top of each arm in each dipole [25]. In this investigation, the inter-element spacing is first kept unchanged with the Connected Dipoles and both are 23.1 mm long. However, the arms of the inter-digital dipole were 0.5 mm shorter than the arms of the Connected Dipole. Thus, the dipole length of the inter-digital dipole was 32.1 mm which is 1 mm shorter than the Connected Dipole. It is notable that 1 mm is 1/30 of the wavelength at the highest frequency, i.e. 10 GHz. Three antenna array models were studied in this analysis. The first model is the inter-digital dipole array with the same element spacing but shorter dipole length and was denoted as "Inter-Digital Dipole Array, D L: 32.1 mm, E S: 23.1 mm".

The second model is made of 33.1 mm long inter-digital dipole, but the inter-element spacing is kept 0.5mm longer than that of the Connected Dipole. Thus, this inter-digital dipole array was designated as ''Inter-Digital Dipole Array, D L: 33.1 mm, E S: 23.6 mm'', and this structure is shown in Fig.6. The third model is the connected dipole Array with length and space of 33.1 mm and 23.1 mm respectively.
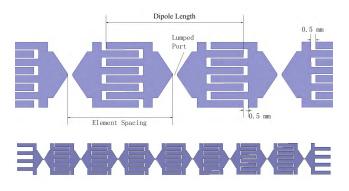

FIGURE 6. The configuration of traditional inter-digital dipoles in a 1×8 linear array, where the top is the detailed dimensions of the antenna element.
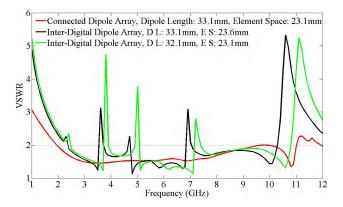

FIGURE 7. The VSWR of the Connected Dipole Array, the same length inter-digital dipole array and the same space inter-digital dipole array.

The array of Connected Dipoles and two interdigital dipole arrays are all placed on the top of a ground plane at distance (t) of 12.9mm. The hyperbolic baluns were not included in these simulations and the three linear arrays were all excited by the ideal lumped port with port impedance 150 Ω, so that the impedance variations of only the linear dipole arrays (radiation aperture) in three cases were studied. The radiation resistance of the array was in the range of 100∼200 Ω [9]. The dipoles in three cases were all excited with the same lumped port at their feeding points. The solution frequencies were all set to be 12GHz in three cases for simulation accuracy. The predicted VSWRs of the central element of the 1×8 linear arrays for the three cases are shown in Fig. 7. As can be observed, the VSWR for two inter-digital dipole arrays were almost the same in the whole frequency band between 1 to 12 GHz, especially on the lower half of the frequency

band. Also, several spikes can be noticed across this band and the VSWR value higher than 2 at these spikes. In contrast to this, the VSWR for the proposed Connected Dipole Array is much lower than that of the two InterDigital Dipole Arrays on 1∼3GHz. Particularly, the VSWR for the Connected Dipole Array is 3.0 at 1 GHz, but the VSWR for the two InterDigital Dipole arrays reached 4.9 and 5.2 at 1 GHz. It is noticeable that the VSWR for the Connected Dipole Array is better than 2 and also smoother than the others over the desired operating frequency band.

This comparison clearly exhibits the improvement on the VSWR level of the Connected Dipole Array in the lower frequency band. The frequency limit of the Connected Dipole Array on the higher frequency band is the onset of the grating lobe in the radiation pattern. Smaller inter-element spacing can move grating lobe onset frequency to higher frequency and even out of the operating band. But small element space will increase the VSWR on the lower frequency band. These observations have led to the conclusion that the Connected Dipole Array has a lower VSWR level on the lower frequency band than the same size inter-digital dipole array.

B. HYPERBOIC MICROSTRIP BALUN

As the port impedance of the planar dipole array element is around 150 Ω across the operating band, the hyperbolic balun is required to connect this element port with any standard 50 Ω microwave circuitry including SMA connector and RF coaxial cable. This balun acts as an impedance transformer to gradually transform the impedance of 150Ω to the characteristic impedance of a coaxial cable, 50Ω. Fig.3 shows the geometry of the differentially fed microstrip balun that was proposed to meet this design goal. This balun is comprised of two metallic strips, namely, the top strip 'v' and the ground strip 'w', where the parameters 'v' and 'w' represent the exponents in the hyperbola curve equation [23]. The top strip 'v' is connected to the inner conductor of the SMA and the ground strip 'w' is connected to the outer conductor. Both the two strips 'v' and 'w' are composed of two symmetrical hyperbolas. The hyperbolas can be expressed in a function of sizes, as in

$$z = \frac{A}{y^v} + B \qquad (1)$$

$$A = \frac{t}{2^v \left(\frac{1}{b^v} - \frac{1}{u^v} \right)} \qquad (2)$$

$$B = \frac{t}{\frac{b^v}{u^v} - 1}. \qquad (3)$$

In HFSS simulator, the excitation of wave port on strip 's' and 'cc' acts as a 50Ω semi-infinite microstrip feed line, and thus the sizes 's' and 'cc' should give a characteristic impedance 50Ω. This can be estimated by using a microwave line calculator. 'k' is the width of the stripline and it can be predicted by using parallel stripline calculator. The impedance transformer design philosophy is as followings: finding the sizes of the balun with the help of computer

optimum program to give a VSWR level <2.0 on the bandwidth of 2~10GHz. Thus, if we replace the 50Ω semi-infinite microstrip feed line with a 50Ω semi-infinite coaxial cable, the VSWR level will not change.
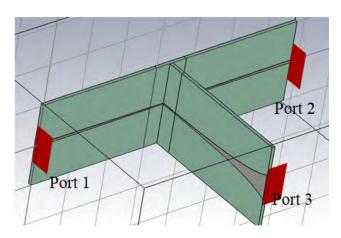

FIGURE 8. Hyperboic microstrip balun design model for performance prediction.

Fig.8 shows the simulated balun model which is designed to predict the phase difference between the two terminals of the output port. As can be seen, it consists of three identical balun models which are interconnected to form a T-shaped structure. By calculating the phase S_{31} minus phase S_{32}, the phase difference can be found. To investigate the S-parameters of the balun, the middle balun of this model was removed, so that only two of the balun are back-to-back connected. Moreover, to predict the output impedance, only one balun was modelled with wave port as input port and lumped port (discrete port) as an output port.
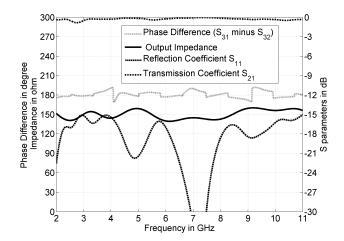

FIGURE 9. Simulated S-parameters, phase difference and output impedance results.

Fig.9 describes the phase difference, S-parameters and the output impedance of the proposed balun. As can be noticed, the phase difference and output impedance are nearly 180 degrees and 150 ohm respectively, while the reflection

coefficient and the transmission coefficient are better than −15 dB and −0.5 dB respectively.
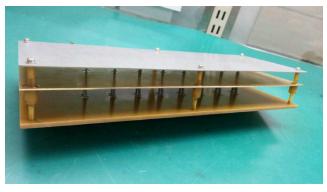

FIGURE 10. The prototype of the 1×8 linear phased array with the proposed balun.

Fig.10 shows the prototype of the proposed phase array antenna with baluns. As can be observed, the right end of the microstrip balun is connected to the port of a dipole and the connected dipoles are placed at distance 't' over a metallic Ground Plane in order to prevent the backward radiation and enhance the forward radiation Gain. It is also clearly noticed that the Connected Dipoles were printed on the reverse side of the upper sheet, the middle sheet is the Ground Plane for the whole array antenna, and the downmost sheet is used to support the whole antenna structure and the SMA Connector is fixed on the backside of this sheet.

FIGURE 11. Reversed version of Figure 10.

To further illustrate how the baluns were connected with the antenna array elements, Fig.11 depicts a rectangular hole is carved on the ground plane in order to let the baluns go through. The balun does not touch the metallic ground plane and thus the ground plane acts as a third independent conductor with the reference voltage potential 0V. This results no electric current flows onto the ground plane, and thus, this contactless structure avoids the current loop mode resonance produced by the electric loop current on the dipole arms and on the ground plane [16]. The loop mode resonance could deteriorate the VSWR on the lower half of the frequency band. The balun is then connected to the SMA on the reverse side of a dielectric sheet, which is used to fix the balun, the Dipole sheet and the Groundsheet.
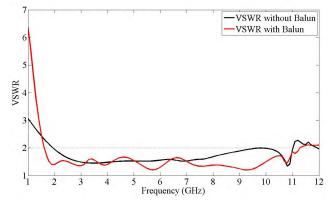
FIGURE 12. The VSWR of the Connected Dipole Array with and without balun on 1~12 GHz bandwidth.

The Connected Dipole Array with microstrip balun and Ground Plane was modeled and simulated in HFSS and CST for cross verification. Fig. 12 compares the VSWR results of the proposed array antenna with and without the balun. It was found that the VSWR level is below 2.0 on the bandwidth 2~11GHz for both cases. Numerical results also show that the introducing balun with the antenna array could further decrease the VSWR level on the desired operating frequency band.

TABLE 2. Onset frequency of grating lobe.

Scan Angle in E-Plane	Onset Frequencies (GHz)
Broadside Radiation	12.98
±15° from the Broadside	10.31
±30° from the Broadside	8.65
±45° from the Broadside	7.60
±60° from the Broadside	6.95

C. THE LIMITATION OF GRATING LOBES ON HIGH FREQUENCY BAND

The frequency limit on the higher band is due to the emergency of the grating lobe effect. By knowing inter-element spacing is 23.1 mm, and the onset frequency of grating lobes for the phased array can be calculated and shown in Table 2. These onset frequencies were calculated simply from the formula found in [9] and [10], which disregards the actual shape of array elements and assumes them as point sources. When the frequency is close, but not equals, to the onset frequency of the grating lobe, the sidelobe level increases. Thus the operating bandwidth is narrower than the frequencies in Table 2. For the broadside radiation, the grating lobe emerges at 12 GHz, while for ±60° scan case, the grating lobe emerges at 6.9 GHz.

Moreover, Table 2 also demonstrates the grating lobe onset frequencies for different scan angles in E-Plane scanning. When a planar phased array is scanning in the D-Plane with both E- and H-Plane element spacing at 23.1mm, it is noticeable that the onset frequencies of grating lobe for each scan angle is higher than the onset frequencies. Thus, in a planar phased array design, if the array is free of grating
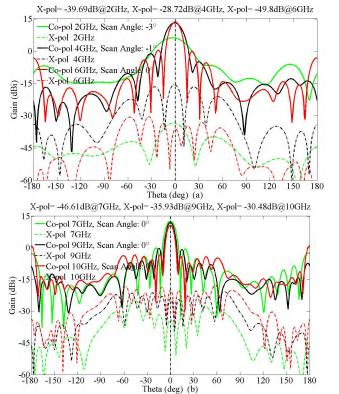

FIGURE 13. Co- and X-Polarized Gain of the 1×8 Connected Dipole Array with balun and groundplane in E-plane for broadside radiation. (a) Low frequency band (2GHz, 4GHz & 6GHz). (b) High frequency band (7GHz, 9GHz & 10GHz).

lobe in E- and H-Plane scanning, there will be no grating lobes in D-Plane scanning. Hence, the array can scan to larger angle without grating lobe in D-Plane than scan angle in E- and H-Planes.

IV. NUMERICAL RESULTS OF 1×8 LINEAR PHASED ARRAY

Prior to constructing the practical prototype, the proposed antenna array of 8 elements was modelled in HFSS and CST software for predicting its overall performance and cross-validation. In the HFSS simulated model, a vacuum box was used to truncate the unbounded computation domain of the design and the antenna was placed in the center of this box.

To reduce the reflection, radiation absorbing boundary was applied to the six surface of the box and the distance between the array and the radiation boundary is larger than 1/4 wavelength at the lowest frequency. In this analysis, the far field Gain for E-Plane at 0°, 30°, 45° and 60° scan on the frequency band 2~10GHz will be presented and discussed as well as cross-polarized gain.

A. CO- AND X-POLARIZED GAIN FOR BROADSIDE RADIATION

Fig.13 shows the co- and cross-polarized gain of the proposed antenna in the E-plane. As can be observed, the gain of the
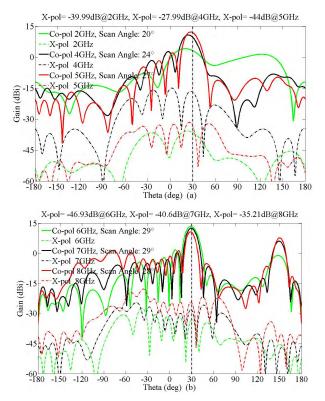
FIGURE 14. Co- and X-Polarized Gain of the 1×8 Connected Dipole Array with balun and groundplane in E-plane, with scan angle 30°. (a) Low frequency band (2GHz, 4GHz & 5GHz). (b) High frequency band (6GHz, 7GHz & 8GHz).

FIGURE 15. Co- and X-Polarized Gain pattern of the 1×8 Connected Dipole Array with balun and groundplane in E-plane, with scan angle 45°. (a) Low frequency band (2GHz, 3GHz & 4GHz). (b) High frequency band (5GHz, 6GHz & 7GHz).

main beam is around 13 dBi over 4 to10 GHz, and is about 5 dBi on 2GHz.

The loss of gain on high frequencies is due to the distance ('t') between the planar Connected Dipoles and the ground plane which is 12.9 mm and equivalent to a quarter of a wavelength at 5.55 GHz. On the higher end of the frequency band, λ shrinks and 't' becomes longer than quarter-wavelength. Thus, the gain of the main beam decreases. This reason is also valid for decreasing gain for other scan angles at a higher frequency. In addition, these results also suggest the Connected Dipole array exhibits good cross-polarization performance. As can be seen, the cross polarization level and side lobe level are less than −28.72dB and −10 dB over the desired frequency band from 2 to 10GHz respectively.

B. CO- AND X-POLARIZED GAIN FOR E-PLANE SCAN

In this study, the eight antenna elements in the array were feed with equal amplitude excitations and progressing phases with the same phase difference, leading to a scanning of the mainbeam. The co- and cross-polarized gain in E-Plane with the mainbeam scanning to 30°, 45° and 60° are given in Fig. 14, 15 and 16, respectively.

For the 30° scan case, the main lobe points to +30° as shown in Fig.14. It is noticeable that another mainlobe appears at θ = 150° due to back radiation as the ground plane is discarded at higher frequencies. However, this mainlobe becomes the sidelobe when the ground plane is presented.
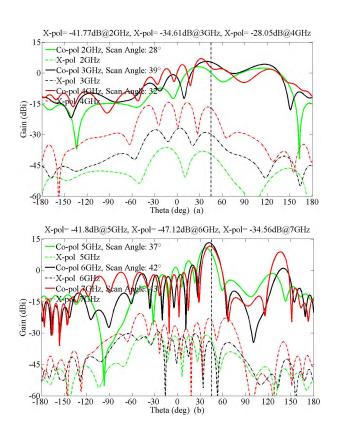
This can be attributed to the limiting size of the ground plane and the rectangular holes on it which permit radiation behind the ground. It is also clearly seen that these sidelobes and the mainlobes are always symmetric around the array plane for all scan angles, and the sidelobe locates at 150°, 135° and 120° for 30°, 45° and 60° scan, respectively. To reduce the sidelobes, it is suggested to use the smaller hole and larger ground plane. This leading to the conclusion that 30° scan case the cross-polarization level is less than −28 dB across the frequency band from 2 to 8 GHz.

For the 45° scan case, the main lobe ought to point to +45° in the E-Plane as illustrated in Fig.15. As can be observed the main beam deviates to smaller scan angles. This deviation is due to the maximum gain of the connected dipole element, which points to 0°, and the array factor of this array is not strong enough. Thus the deviation of the main lobe tends to greatly decrease when a larger array with more elements is used. In this case, it is found that operating band is from 2 to7 GHz with −12 dB sideobe levels and the cross-polarization level is less than −28 dB.

In the case of 60° scan, the main lobe points to +60° in the E-Plane, as depicted in Fig.16. As can be seen, the sidelobe levels are better than −9dB for all the frequencies except at 5 GHz it increases to −5 dB. It is also found that at this scan angle the operating band is from 2 to 6.5 GHz with cross polarization level less than −25 dB.
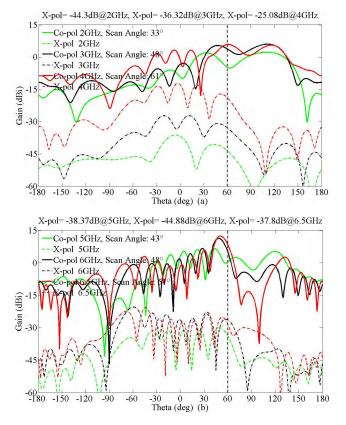
X-pol= -44.3dB@2GHz, X-pol= -36.32dB@3GHz, X-pol= -25.08dB@4GHz

X-pol= -38.37dB@5GHz, X-pol= -44.88dB@6GHz, X-pol= -37.8dB@6.5GHz

FIGURE 16. Co- and Cross-Polarized Gain pattern of the 1×8 Connected Dipole Array with balun and groundplane in E-plane, with scan angle 60°. (a) Low frequency band (2GHz, 3GHz & 4GHz). (b) High frequency band (5GHz, 6GHz & 6.5GHz).

FIGURE 17. The 1×8 phased array was fed with a 8:1 power divider.

FIGURE 18. Measured and simulated VSWR of the central element and edge element in 1×8 phased array.

V. MEASURED RESULTS OF 1×8 LINEAR PHASED ARRAY

To verify the proposed theoretical model, a 1×8 linear phased array prototype was constructed and measured in the 39th Research Institute of China Electronics Technology Group Corporation as shown in Fig.17. The array prototype was only tested for broadside radiation, and the 8 elements were all fed with equal amplitude and no phase difference. Fig.18 compares the simulated and measured VSWR results at the central element and edge element in the array. It is found that VSWR at the edge elements is greater than 2 at the frequency band between 2 to 3 GHz. This is due to the different structure of the arms of the edge dipole. As for the six identical and symmetrical armed dipole, the VSWR is less than 2.0 over the desired frequency band, i.e. 1.8∼11.8GHz. In general, both theoretical and experimental results are in good agreement. Some discrepancies of the results are due to the fabrication errors.

The simulated and measured E-Plane co- and cross-polarized gain were normalized to the highest value of the co-polarized gain, and were plotted in Fig.19 at various frequencies, i.e. 1.5 GHz, 2 GHz, 3 GHz, 4 GHz, 5 GHz, 6 GHz, 7 GHz, 8 GHz, 9 GHz and 9.5 GHz for better comparison As can be observed, the measured co-polarized gains match the simulated co-polarized gains well, but the measured cross-polarized gains are much higher than the simulated cross-
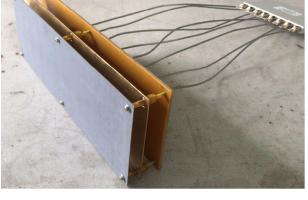
polarized gains. The measured cross polarization levels of the main beam are clearly indicated on each of the figure and these values are varying from −0.99 dB to −43.35 dB at different frequencies. In addition, the sidelobe levels for co-polarized gain are less than −10dB across the 2 to 9 GHz band for broadside radiation.

VI. FEED BLINDNESS IN AN INFINITE SINGLE POLARIZED PLANAR ARRAY WITH HYPERBOLIC MICROSTRIP BALUN

Scan blindness was reported in the E-Plane scan of a planar array antenna which is constituted by a Tightly Coupled Dipole Array [16], [21], [30], [31]. Scan blindness leads to null on the scanned main beam on certain scan angle at a certain frequency. In the case of Connected Dipole Array, the scan blindness is mainly caused by the Surface Waves Blindness and the Feed Blindness which is also called the Common Mode Resonance. The Surface wave blindness is caused by the freestyle surface waves propagating in the dielectric layers in the vicinity of the connected dipoles. If the dielectric layer close to the dipoles has low relative permittivity ε_r and very thin thickness, there are no freestyle surface waves that support Surface Wave blindness [10]. The dielectric constant of ε_r of the substrate used in the
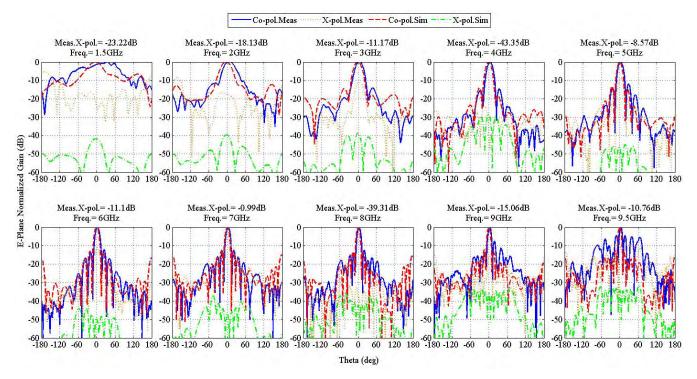
FIGURE 19. E-Plane normalized co- and cross-polarized gain of the 1×8 linear array prototype at 1.5 GHz, 2 GHz, 3 GHz, 4 GHz, 5 GHz, 6 GHz, 7 GHz, 8 GHz, 9 GHz, and 9.5 GHz for broadside radiation. Both measured and simulated gain are presented.

proposed design is 2.2 and the thickness of the dielectric layer is only 1mm, thus the proposed connected dipole array does not support Surface Wave blindness. Based on this, it can be concluded that the scan blindness is only caused by the Feed Blindness.

In this section, the feed blindness of an infinite planar array of a single polarized connected dipole array is studied. In the design model, only single element of the proposed antenna array was used and the boundary condition is set with the periodic master and slave boundaries in both E- and H-Plane to simulate an element in an infinite planar array. In this analysis, the scan angles were selected to be broadside, i.e. ±15°, ±30°, ±45°, and ±60°. The E-Plane scanning will start first, then it follows by the H- and D-plane scanning. According to the simulated results which are presented in Table 3, there is no Feed Blindness of the single-polarized infinite planar array at scan angles of broadside, i.e. at ±15°, and −30° radiation in E-Plane on the frequency band of 2∼10GHz. But it appears for scan angles at +30°, ±45°, −60°, and +60° E-Plane radiation, the Feed Blindness manifests itself at 4.2GHz, 4.9GHz, 5.9GHz, and 6GHz, respectively. Other than these frequency points, the radiation of the infinite planar array shows no Feed Blindness on the bandwidth of 2∼10GHz for each scan angle in E-Plane. From the observation above, the Feed Blindness frequency increases as the E-Plane scan angle increases. It should be noted that the Feed Blindness frequency for positive E-Plane scan angle and negative E-Plane scan angle are not the same.

TABLE 3. Scan blindness frequency for different scan angles (PEC pins).

Scan Angles (deg)	Left Side (GHz)	Right Side (GHz)	Both Sides (GHz)	No PEC Pins (GHz)
0°	None	None	None	None
+15°	3.7 & 5.4	None	None	None
-15°	None	None	None	None
+30°	4.0 & 5.5	4.0	3.9 & 5.9	4.2
-30°	None	5.6	None	None
+45°	4.4 & 5.8	4.4	4.3 & 6.6	4.9
-45°	4.4	5.9	None	4.9
+60°	4.8 & 6.6	4.9 & 6.5	4.6	6.0
-60°	6.6	None	None	5.9

Fig.20 illustrates the Feed Blindness is caused by the cancellation between the radiation of the dipole and that of the balun [22]. Ideally, the currents on the top strip and the Ground strip of the balun should be Differential Mode Currents, i.e. equal magnitudes and opposite direction (180° phase difference). There will be no net current on the ideal balun and thus the balun does not radiate. However, the currents on both strips of the balun are not always equal in magnitudes on all of the frequencies, and a net current along the balun, perpendicular to the array plane, is shown
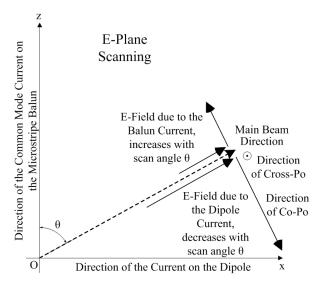
FIGURE 20. Common Mode Current on Balun contributes to the Co-Polarization level in E-Plane scanning, results to Feed Blindness at certain scan angle *θ* on certain frequency.

FIGURE 21. Common Mode Current on Balun contributes to the Cross Polarization level in H-Plane scanning, results to an increasing X-Pol level with larger scan angle *θ*.

as in Fig. 20 [33]. This net current along the balun is named as Common Mode Current. On the low-frequency end of this design, i.e. 2∼4.27GHz, when the length of Balun plus the length of half of the dipole is less than half of the wavelength (λ/2), the Common Mode Current and the Dipole Current have the direction as depicted in Fig.20. As can be noticed, both the Dipole current and the Common Mode Current produce E-Field orthogonal to the direction of the main beam. In the far field region, the E Field component along the beam direction is diminished to zero, and the component orthogonal to the beam direction becomes the dominant E vector. This dominant E field due to either the Dipole or the Balun is cancelled by each other. Notably, when the array scanned to large angles, the Dipole E Field decreases but the Balun E Field increases, thus, at certain scan angle and frequency, the Dipole E Field will be cancelled completely by the Balun E Field, and the antenna array gives the Feed Blindness. However, when the array is scanned to negative angles i.e. −θ, the dominant E Fields due to the Dipole and the Balun do not cancel each other, and there will be no scan blindness for all of the negative scan angles at a low frequency band, such as 2∼4.27GHz in this design. This is the reason why the Feed Blindness frequencies for ±θ are not the same. In addition, it is interestingly found the infinite planar array does not have Feed Blindness for all the negative scan angles below 4.27GHz as shown in Table 3.

As shown in Fig.20, the common mode current has no influence on cross-polarized E field. Thus, the X-Pol level in E-Plane scanning remains rather low with larger scan angle *θ*. When the frequency goes up and the wavelength decreases, the common mode current direction on the balun will point downward. The situation is different on low frequency band. But Fig.20 does give a clear explanation on how the balun radiation interacts with the Dipole radiation.
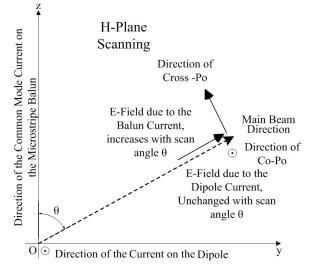
Fig.21 demonstrates the concept of when the planar array is scanned in H-Plane, the orthogonal common mode current on the balun does not increase or decrease the level of the co-pol E Field. In other words, there is no Feed Blindness in H-Plane scanning. This concept can be confirmed by both the simulation results and other published work [9]–[13]. The Feed Blindness only exist when the planar array with Microstrip Balun is scanned in the E-Plane [16], [21]. However, the common mode current contributes to the level of the Cross-Polarized E Field. With the scan angle *θ* increasing, the cross polarization level increases accordingly.

Considering the case of D-Plane scan, the common mode current affects both the co-pol and the cross-pol E Fields. However, this influence caused by the balun's common mode current on the co-pol E Field is not as strong as the case in E-Plane scan; thus, the co-pol E Field tends not to be cancelled completely and Feed Blindness does not appear. With an increasing scan angle *θ*, it is believed that the co-pol E Field level will decrease and the cross-pol E Field level will increase, thus results in a higher level of the cross-polarization.

In short, it is the radiation of the balun, caused by the common mode currents, that leads to Feed Blindness in E-Plane scan and high cross-polarization level in H- and D-Plane scan. If the balun does not radiate, there will be no Feed Blindness for all the positive and negative scan angles in E-Plane scanning and the cross polarization level in H-Plane scanning is also decreased. In order to verify this, the balun was removed in the infinite planar array, and the dipole was excited with an ideal lumped port with a port impedance of 150Ω. This ensures that the radiation of the balun does not occur. The simulation results confirm that no Feed Blindness on the band of 2∼10GHz for all scan angles: broadside, at angle of ±15°, ±30°, ±45°, and ±60°

in E-Plane. And the cross polarization level in H-Plane scanning also decreased significantly.

In order to prevent the radiation of the vertical common mode currents on the balun, cable organizers were proposed to shield the balun radiation [12]. But the cable Organizers were three-dimensional metallic structures that are bulky and difficult to assembly. Moreover, Cable Organizers are not easy to be scaled to very high frequency [16]. Thus, other ways that prevent the scan blindness in connected dipole arrays were proposed. They are adding vertical Perfect Electric Conductor (PEC) pins or walls at the vicinity of the problematic balun. The PEC pins and walls near the balun change the radiation property of the common mode current so that the Feed Blindness frequency is eliminated accordingly.

A. THE METHOD OF CHANGING FEED BLINDNESS FREQUENCY: E-PLANE PEC PINS

In order to remove the Feed Blindness out of the desired frequency band, PEC pins were first introduced in the array element as illustrated in Fig. 22, [16], [21]. The PEC pins with a diameter of 0.6 mm, and height of 13 mm were added along the center line of the connected dipole and were symmetrical around the balun. The distances between the PEC pins and the center of the balun are 2.55mm. The PEC pins contact the PEC ground plane but do not touch the connected dipole to prevent the electric current of the balun from flowing onto the PEC pins and the ground plane. The latter two can form a loop antenna which can also resonant at some low frequency in the bandwidth, as referred to as low-frequency loop resonance [16], [21].
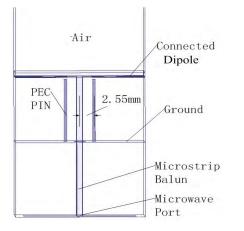

FIGURE 22. Two PEC Pins located symmetrically on the 2 sides of the Microstrip Balun. E-Plane View.

In order to comprehend the effectiveness of introducing PEC pins into the antenna design, there are four models, i.e. only left side PEC pin, only right side PEC pin, both PEC pins and without PEC pin, from Fig.22 are proposed for this study. Table 3 demonstrates the feed blindness frequencies for these four models for different scan angles on the frequency band from 2 to10 GHz.

From Table 3, it is observed that the introduction of PEC pins can change the feed blindness frequency. However, the number of feed blindness frequencies increase for some scan angles. For instance, there are 2 feed blindness frequencies for scan angles of +15°, +30°, +45°, and +60°.

B. THE METHOD OF CHANGING FEED BLINDNESS FREQUENCY: H-PLANE PEC WALLS

In Table 3, it is clearly shown that PEC pins do change the Feed Blindness frequencies, but this method also complicates the situation by introducing more Feed Blindness frequencies. To combat this problem, two PEC walls were proposed to add symmetrically in H-Plane on both sides of the balun, as depicted in Fig.23. For convenient comparison of the case of PEC pins, the PEC Walls was also located at 2.55mm from the center of the balun, so the position of the PEC walls and the PEC pins are the same. In this investigation, again four models were constructed, i.e. only left side PEC wall, only right side PEC wall, both side PEC walls and without PEC wall, were studied on the frequency band of 2~10GHz, and in the scan angle of −60°~0°~+60° in the E-Plane, as shown in Fig.23.

FIGURE 23. Two PEC Walls located symmetrically on the 2 sides of the Microstrip Balun. D-Plane View.

Table 4 elucidates the feed blindness frequencies for all the models. From Table 4, the first observation is that although the PEC Walls cannot remove the Feed Blindness frequency out of the desired operating band, the PEC walls do change the Feed Blindness frequencies to other frequency points. The second observation is that in contrast to PEC pins, the PEC walls do not introduce new Feed Blindness frequency point to the desired frequency band. For the three cases with PEC wall in Table 4, there is only one Feed Blindness frequency point on the band of interest, i.e. 2~10GHz, for each scan angle, while there are two Feed Blindness frequency points on the case of PEC Pins for some scan angles. The third important observation is that the Feed Blindness frequency decreases as the scan angle decreases. This observation gives a good indication that if moving the 60° Feed Blindness frequency below 2GHz or the lower end of the

TABLE 4. Scan blindness frequency for different angles (PEC walls).

Scan Angles (deg)	Left Side (GHz)	Right Side (GHz)	Both Sides (GHz)	No PEC Walls (GHz)
0°	None	None	None	None
+15°	3.2	None	3.2	None
-15°	None	None	None	None
+30°	3.3	3.4	3.3	4.2
-30°	None	None	None	None
+45°	3.5	3.6	3.5	4.9
-45°	7.0	None	4.3	4.9
+60°	3.8* (End-Fire for 2~3.4)	3.8* (End-Fire for 2~3.4)	3.7	6.0
-60°	None* (End-Fire for 2~3.4)	None* (End-Fire for 2~3.4)	4.4	5.9

TABLE 5. +60° scan blindness frequency of both sides PEC walls/pins for different distances between walls/pins and balun.

Distance (mm)	+60° Scan blindness Frequency (GHz) PEC Walls on Both Sides	+60° Scan blindness Frequency (GHz) PEC Pins on Both Sides
No PEC Wall and PEC Pin	6.0	6.0
2.55	3.7	4.6
4.05	3.2	4.1
4.55	3.1	4.0
11.55	2.9	3.75

2.9 GHz, remaining above 2 GHz. As to both sides PEC Pins case, the same trend was also observed but the Feed Blindness frequency is not the same as that in the case of both sides PEC walls case. The Feed Blindness frequency decreases when the distance between the PEC pins and the center of the balun increases as observed in Table 5.

In order to prove the aforementioned finding, the single polarized infinite planar array with PEC walls on both sides of the balun at distance 11.55mm was modeled in HFSS. The numerical results verified this and a phased array free of Feed Blindness with scan volume of ±60° on the bandwidth of 2.9~6.95 GHz was presented. When the scan volume shrinks to lower scan angle, the Feed Blindness frequency also decreases to lower frequency, as shown in Table 6. It should be highlighted that the array without any PEC wall and PEC pin were also given in Table 6 for comparison.

TABLE 6. Scan blindness frequency of both sides PEC walls/pins at the largest distance for different scan angles.

Scan Angles (deg)	PEC walls on Both Sides (GHz)	PEC pins on Both Sides (GHz)	No PEC wall and PEC pin (GHz)
0°	None	None	None
+15°	2.6	None	None
-15°	None	None	None
+30°	2.7	3.4 & 6.7	4.2
-30°	None	None	None
+45°	2.8	3.6 & 7.4	4.9
-45°	None	7.4	4.9
+60°	2.9	3.7	6.0
-60°	None	None	5.9

frequency band, then a planar connected dipole array free of Feed Blindness in scan volume of ±60° on desired frequency band is devised.

Noticeably, in the general array antenna, the area of the ground plane is usually larger than the area of the dipole array aperture in order to prevent backward radiation. In the simulation model in HFSS, the ground plane was set to be infinite ground plane boundary condition to simulate the general case in which the ground plane is larger than the dipole aperture. With this boundary setting, the change in the radiation pattern of the infinite planar array was observed. When the planar array is operating on the lower end of the frequency band, such as 2~3.4GHz; and the scan angle is very large, e.g. E-Plane ±60° scan, corresponding to the cases with the asteroid '*' in Table 4, the radiation pattern exhibits a "End-Fire Pattern" for only one PEC Wall added on each side of the balun either Left or Right. But the radiation does not go to end fire in the case of both PEC Walls.

VII. DECREASING FEED BLINDNESS FREQUENCY
In this section, the methods on how to remove the feed blindness frequency of E-Plane ±60° scan out of the desired frequency band will be discussed. This can be done by increasing the distance of the PEC walls. The Feed Blindness frequency decreases as the distance increases, and a planar phased array without feed blindness can be found.

One of the feasible method is to increase the distance between the PEC wall and the center of the balun. The distance range is selected from 0.55mm to 11.55mm due to the physical sizes of this dipole configuration. The feed blindness frequencies of this study are predicted and shown in Table 5 for E-Plane +60° scan. For better comparison, both PEC walls and PEC pins on both sides were selected. As can be seen, the eed blindness frequency decreases as the distance increases. However, when the distance reach its extremity of 11.55mm, the feed blindness frequency reaches

The PEC pins at the largest distance on both sides of the balun was also presented in Table 6. As proved before, the Feed Blindness frequency decreases as the scan angle (absolute value) decreases. However, the PEC pins case is more complicated than the PEC walls case. There are two frequency points (a lower frequency point and a higher one) supporting the Feed Blindness on some scan angles

TABLE 7. Comparison between this work and other ultra-wideband phased array.

Design	Bandwidth	Scan Volume		Max VSWR	Polarization	WAIM Superstrate		Total Height (λ_{low})	Planar dipole Aperture
		E-Plane	H-Plane			ε_r	Thickness (λ_{low})		
This work	2:1 (3~6 GHz)	±60°	±60°	2.0	Linear	N/A	0.0	0.23 @2GHz	Yes
TCDA Integrated Balun [28]	6.3:1 (0.69~4.37GHz)	±45°	±45°	2.65	Linear	1.7	0.03	0.15	Yes
TCDA Twin Wires Balun [27]	1.56:1 (8~12.5GHz)	±70°	±60°	2.0	Linear	1.7	0.17	0.33	Yes
Octagonal Ring Array [29]	4.4:1 (2.5~11GHz)	±45°	N/A	1.82	Linear	0.0	0.07	0.43	Yes
Vivaldi Array [26]	8:1 (1~8GHz)	±45°	±45°	2.0	Dual Linear	N/A	0.0	0.43	No

(+30° and +45°). The lower Feed Blindness frequency point decreases as the distance between the balun and PEC pins increases, which is also held true in PEC walls case. But the higher Feed Blindness frequency point increases as the distance increase, which does not exist in the PEC walls case.

For both cases, the Feed Blindness frequency points for positive and negative scan angles are generally not the same because the microstrip balun is not symmetric. The balun ground is on the left side but the balun strip is on the right side. Based on all the above design principles, an ultra-wideband single polarized infinite planar phased array with ±60° scan volume on E-, H-, and D-Plane on the bandwidth of 3~6GHz without Feed Blindness was proposed.

VIII. CONCLUSION

A 1×8 linear single polarized phased array with connected dipoles was simulated and measured. The frequency band and E-plane scan range are 2~9 GHz for broadside radiation, 2~8GHz for ±30° scan, 2~7 GHz for ±45° scan, and 2~6.5GHz for ±60° scan. The measured VSWR for broadside radiation is less than 2.0 across 1.8~11.8 GHz frequency band. The connected dipole was total planar, thus it can be made of PCB board. The substrate of the dipoles and baluns was the same material and has 1mm thickness. By implementing low dielectric and thin substrate in the antenna array design, this reduces the surface wave blindness in the scan range and in the frequency band. By comparing the VSWR performance of the proposed connected dipole array and the traditional inter-digital dipole array, the proposed array exhibits a lower VSWR on the low end of the working frequency band. As the input impedance of the antenna array is 150 Ω, an optimized hyperbolic microstrip balun that used to transform the impedance from 50 Ω to 150 Ω was designed. So the antenna can be fed by coaxial cables through SMA connector.

Further, an infinite planar (2D) phased array with the same connected dipoles and baluns was simulated in HFSS. Feed induced blindness was observed only in the E-Plane scan. This feed blindness is caused by the cancellation between the radiation of the dipole and balun. H-Plane PEC walls could move the blindness to a lower frequency. Finally, an infinite planar array without feed blindness in scan volume of ±60° in E-, D-, and H-Plane was designed and simulated in HFSS, and the bandwidth turns out to be 3~6.5GHz.

Finally, the performance of the proposed ultra-wideband phased array antenna is compared with other published works and is presented in Table 7. These works include the Tightly Coupled Dipole Array (TCDA) [27], [28], Tightly Coupled Octagonal Ring Array [29] and the Vivaldi Array [26]. As shown in Table 7, all the published works demonstrate a wide bandwidth performance and a large scan volume. However, TCDAs need a complicated balun to match the antenna impedance to the feed point [14], [28], while the traditional differential balun, i.e. Twin Wires, only supports a narrow bandwidth [27]. Moreover, the TCDAs need a bulky wide angle impedance matching (WAIM) superstrate to be placed onto the radiating dipole aperture with relative permittivity, ε_r, of usually less than 2.0. The dielectrics with ε_r less than 2.0 are rare, expensive and always have ohmic loss, thus reducing the antenna Gain. Conventional Vivaldi Array is not a planar structure, leading to high Cross-Polarization level in D-Plane scan and is difficult to assemble. Notably, the maximum cross-polarization level of the Vivaldi Array is 12 dB higher than the co-polarization level in D-Plane for large scan angles [26]. As for the Octagonal Ring Array, it does not has dielectric superstrate in front of the dipole, thus reducing the total weight of the whole array, but it needs octagonal ring-shaped structure and Frequency Selective Surface (FSS) sheet to be mounted in front of the dipole aperture. Due to this, the assembly for it is still difficult. In the proposed

work, the Connected Dipole Array does not need a bulky dielectric superstrate, and thus the whole phased array can be very light. The whole antenna, including the hyperbolic balun, was made of the same piece of PCB board, thus the cost of making this antenna could be very cheap. The total height of the whole array, only $0.23\lambda_{low}$, which is much smaller than [26], [27], [29]. Therefore, the Connected Dipole array is an attractive candidate for wideband communication and sensing applications, especially on small and low-cost platforms.

ACKNOWLEDGMENT

REFERENCES

[1] M. H. Novak and J. L. Volakis, "Ultrawideband antennas for multiband satellite communications at UHF–Ku frequencies," *IEEE Trans. Antennas Propag.*, vol. 63, no. 4, pp. 1334–1341, Apr. 2015.

[2] W. F. Moulder, K. Sertel, and J. L. Volakis, "Superstrate-enhanced ultrawideband tightly coupled array with resistive FSS," *IEEE Trans. Antennas Propag.*, vol. 60, no. 9, pp. 4166–4172, Sep. 2012.

[3] G. C. Tavik *et al.*, "The advanced multifunction RF concept," *IEEE Trans. Microw. Theory Techn.*, vol. 53, no. 3, pp. 1009–1020, Mar. 2005.

[4] L. Lewis, M. Fassett, and J. Hunt, "A broadband stripline array element," in *Proc. Antennas Propag. Soc. Int. Symp.*, 1974, pp. 335–337.

[5] D. H. Schaubert, A. O. Boryssenko, M. N. Vouvakis, G. Paraschos, W. Elsallal, and S. Kasturi, "Wide bandwidth arrays of vivaldi antennas," in *Proc. Inst. Eng. Technol. Seminar Wideband, Multiband Antennas Arrays Defence Civil Appl.*, London, U.K., 2008, pp. 1–20.

[6] S. Sugawara, Y. Maita, K. Adachi, K. Mori, and K. Mizuno, "A mm-Wave tapered slot antenna with improved radiation pattern," in *IEEE MTT-S Int. Microw. Symp. Dig.*, Denver, CO, USA, vol. 2, Jun. 1997, pp. 959–962.

[7] H. Holter, T.-H. Chio, and D. H. Schaubert, "Elimination of impedance anomalies in single- and dual-polarized endfire tapered slot phased arrays," *IEEE Trans. Antennas Propag.*, vol. 48, no. 1, pp. 122–124, Jan. 2000.

[8] Y. Zhang and A. K. Brown, "Bunny ear combline antennas for compact wide-band dual-polarized aperture array," *IEEE Trans. Antennas Propag.*, vol. 59, no. 8, pp. 3071–3075, Aug. 2011.

[9] B. A. Munk, *Finite Antenna Arrays and FSS*. Hoboken, NJ, USA: Wiley, 2003.

[10] B. A. Munk, *Frequency Selective Surfaces: Theory and Design*. Hoboken, NJ, USA: Wiley, 2000.

[11] B. Munk *et al.*, "A low-profile broadband phased array antenna," in *Proc. IEEE Antennas Propag. Soc. Int. Symp.*, vol. 2, Jun. 2003, pp. 448–451.

[12] M. Jones and J. Rawnick, "A new approach to broadband array design using tightly coupled elements," in *Proc. Mil. Commun. Conf.*, 2007, pp. 1–7.

[13] S. S. Holland, D. H. Schaubert, and M. N. Vouvakis, "A 7–21 GHz dual-polarized planar ultrawideband modular antenna (PUMA) array," *IEEE Trans. Antennas Propag.*, vol. 60, no. 10, pp. 4589–4600, Oct. 2012.

[14] J. P. Doane, K. Sertel, and J. L. Volakis, "A wideband, wide scanning tightly coupled dipole array with integrated balun (TCDA-IB)," *IEEE Trans. Antennas Propag.*, vol. 61, no. 9, pp. 4538–4548, Sep. 2013.

[15] H. A. Wheeler, "Simple relations derived from a phased-array antenna made of an infinite current sheet," *IEEE Trans. Antennas Propag.*, vol. AP-13, no. 4, pp. 506–514, Jul. 1965.

[16] S. S. Holland and M. N. Vouvakis, "The planar ultrawideband modular antenna (PUMA) array," *IEEE Trans. Antennas Propag.*, vol. 60, no. 1, pp. 130–140, Jan. 2012.

[17] E. Yetisir, N. Ghalichechian, and J. L. Volakis, "Ultrawideband array with 70 ° scanning using FSS superstrate," *IEEE Trans. Antennas Propag.*, vol. 64, no. 10, pp. 4256–4265, Oct. 2016.

[18] J. J. Lee, S. Livingston, R. Koenig, D. Nagata, and L. L. Lai, "Compact light weight UHF arrays using long slot apertures," *IEEE Trans. Antennas Propag.*, vol. 54, no. 7, pp. 2009–2015, Jul. 2006.

[19] A. Neto and J. J. Lee, "Ultrawide-band properties of long slot arrays," *IEEE Trans. Antennas Propag.*, vol. 54, no. 2, pp. 534–543, Feb. 2006.

[20] J. J. Lee, S. Livingston, and D. Nagata, "A low profile 10:1 (200–2000 MHz) wide band long slot array," in *Proc. IEEE Antennas Propag. Soc. Int. Symp.*, San Diego, CA, USA, Jul. 2008, pp. 1–4.

[21] S. S. Holland and M. N. Vouvakis, "The banyan tree antenna array," *IEEE Trans. Antennas Propag.*, vol. 59, no. 11, pp. 4060–4070, Nov. 2011.

[22] J.-P. R. Bayard, D. H. Schaubert, and M. E. Cooley, "E-plane scan performance of infinite arrays of dipoles printed on protruding dielectric substrates: Coplanar feed line and E-plane metallic wall effects," *IEEE Trans. Antennas Propag.*, vol. 41, no. 6, pp. 837–841, Jun. 1993.

[23] T. Xia, S. Yang, and Z. Nie, "Design of a tapered balun for broadband arrays with closely spaced elements," *IEEE Antennas Wireless Propag. Lett.*, vol. 8, pp. 1291–1294, 2009.

[24] B. Riviere, H. Jeuland, and S. Bolioli, "New equivalent circuit model for a broadband optimization of dipole arrays," *IEEE Antennas Wireless Propag. Lett.*, vol. 13, pp. 1300–1304, 2014.

[25] R. He, S. Yang, and Z. Nie, "An planar ultrawideband phased array with low profile impedance matching layers," in *Proc. Int. Conf. Comput. Problem-Solving (ICCP)*, Leshan, China, 2012, pp. 25–28.

[26] R. W. Kindt and W. R. Pickles, "Ultrawideband all-metal flared-notch array radiator," *IEEE Trans. Antennas Propag.*, vol. 58, no. 11, pp. 3568–3575, Nov. 2010.

[27] J. A. Kasemodel, C.-C. Chen, and J. L. Volakis, "Wideband planar array with integrated feed and matching network for wide-angle scanning," *IEEE Trans. Antennas Propag.*, vol. 61, no. 9, pp. 4528–4537, Sep. 2013.

[28] J. P. Doane, K. Sertel, and J. L. Volakis, "A 6.3:1 bandwidth scanning tightly coupled dipole array with co-designed compact balun," in *Proc. IEEE Int. Symp. Antennas Propag.*, Chicago, IL, USA, Jul. 2012, pp. 1–2.

[29] Y. Chen, S. Yang, and Z.-P. Nie, "A novel wideband antenna array with tightly coupled octagonal ring elements," *Prog. Electromagn. Res.*, vol. 124, pp. 55–70, 2012. [Online]. Available: http://www.jpier.org/PIER/pier.php?paper=11121312, doi: 10.2528/PIER11121312.

[30] S. G. Hay and J. D. O'Sullivan, "Analysis of common-mode effects in a dual-polarized planar connected-array antenna," *Radio Sci.*, vol. 43, no. 6, pp. 1–9, Dec. 2008.

[31] R. J. Mailloux, *Phased Array Antenna Handbook* (Artech House Antennas and Propagation Library), 2nd ed. Norwood, MA, USA: Artech House, 2005, pp. 306–319.

[32] A. Ludwig, "The definition of cross polarization," *IEEE Trans. Antennas Propag.*, vol. AP-21, no. 1, pp. 116–119, Jan. 1973.

[33] J. D. Kraus and R. J. Marhefka, *Antennas for all Applications*, 3rd ed. New York, NY, USA: McGraw-Hill, 2002, pp. 297–315.

RUOYU HE was born in Baiyin, Gansu, China, in 1986. He received the B.S. degree in electronic and information engineering from Wuhan University, Wuhan, China, in 2009, and the M.S. degree in electromagnetic field and microwave engineering from the University of Electronic Science and Technology of China, Chengdu, China, in 2013. He is currently pursuing the Ph.D. degree in astronomical technology at the University of Chinese Academy of Sciences, Beijing, China.

From 2013 to 2014, he was a Research Assistant with National Astronomical Observatories, Chinese Academy of Sciences. Since 2015, he has been an Assistant Professor with the Key Laboratory of Lunar and Deep Space Exploration, University of Chinese Academy of Sciences. He has authored two articles and five inventions. His research interests include ultra-wideband phased array, wideband antenna for 5G base station, and high frequency antenna for radio astronomy.

Mr. He is a member of the Chinese Institute of Electronics.

HONGBO ZHANG was born in 1964. He is currently a Professor with the Key Laboratory of Lunar and Deep Space Exploration, Chinese Academy of Sciences, Beijing, China. He is also the Chief Engineer with the Science and Application Center for the Moon and Deep Space Exploration. His research interests include antennas in radio astronomy.

CHAN HWANG SEE (M'14–SM'15) received the B.Eng. degree (Hons.) in electronic, telecommunication and computer engineering and the Ph.D. degree from the University of Bradford, U.K., in 2002 and 2007, respectively. He is currently a Senior Lecturer (Programme Leader) in electrical and electronic engineering with the School of Engineering, University of Bolton, U.K. He is also a Visiting Research Fellow with the School of Engineering and Informatics, University of Bradford. Previously, he was a Senior Research Fellow with the Antennas and Applied Electromagnetics Research Group, University of Bradford. He has published over 180 peer-reviewed journal articles and conference papers in the areas of antennas, computational electromagnetics, microwave circuits, and wireless sensor system designs. He has co-authored one book and three book chapters. His research interests cover wireless sensor network system design, computational electromagnetism, antennas and acoustic sensor design. He is a Chartered Engineer and a member of the Institution of Engineering and Technology. He is also a fellow of the Higher Education Academy. He was a recipient of two Young Scientist Awards from the International Union of Radio Science and the Asia–Pacific Radio Science Conference in 2008 and 2010, respectively. He received a certificate of excellence for his successful knowledge transfer partnership with Yorkshire Water on the design and implementation of a wireless sensor system for sewerage infrastructure monitoring in 2009. He is an Associate Editor for the IEEE ACCESS.

YAN SU received the B.S. degree in electronic engineering from the Shenyang University of Technology, Shenyang, China, in 1997, and the Ph.D. degree in astronomical of techniques and methodology from National Astronomical Observatories, Chinese Academy of Sciences, Beijing, China, and The University of Manchester, Manchester, U.K., in 2003, under the Joint Doctoral Program.

Since 2012, she has been a Professor with National Astronomical Observatories, Chinese Academy of Sciences. Her research interests include the development of downlink ground station for Chinese lunar exploration, ground penetrating radar, and microwave radio meter applications to planetary investigations.

YUE MA was born in Tangshan, Hebei, China, in 1986. She received the bachelor's degree (Hons.) in electrical and electronic engineering from the University of Bradford, U.K., in 2009, and the master's degree (Hons.) in electrical and electronic engineering from the University of Bradford, U.K., in 2010. The research field in mobile and Satellite communication antenna studies that includes RFID passive tag design at Europe UHF band, MIMO mobile handset antenna designs, CPW, UWB, and phase array antennas for wireless communication applications in U.K. Since 2013, she involves in the development on wide band single pixel feed, phased array feed, low noise amplifier, and filter designs for square kilometre array radio telescope with National Astronomical Observatories, Chinese Academy of Sciences. In 2017, she received the Young Scientists Award in the 32nd International Union of Radio Science General Assembly and Scientific Symposium (URSI 2017 GASS).

DEQING KONG was born in Mengyin, Shandong, China, in 1978. He received the B.S. and M.S. degrees in mechanical and electronic engineering from Tianjin University, Tianjin, China, in 2000 and 2003, respectively, and the Ph.D. degree from the Graduate School, Chinese Academy of Sciences, in 2008. His research interests include antenna arraying and deep space communications.

XINYING ZHU was born in 1982. He received the B.S. degree in automation from Tianjin University, Tianjin, China, in 2004, and the M.S. and Ph.D. degrees from the Key Laboratory of Lunar and Deep Space Exploration, National Astronomical Observatories, Chinese Academy of Sciences, Beijing, China. His research interests include radio antenna array, data acquisition system, VLBI observation system, and radio astronomy.

RAED ABD-ALHAMEED (M'02–SM'13) received the B.Sc. and M.Sc. degrees from Basrah University, Basrah, Iraq, in 1982 and 1985, respectively, and the Ph.D. degree from the University of Bradford, West Yorkshire, U.K., in 1997, all in electrical engineering. He has long years' research experience in the areas of radio frequency, signal processing, propagations, and antennas and electromagnetic computational techniques. He has been a Research Visitor with Wrexham University, Wales, since 2009, covering the wireless and communications research areas. He is currently a Professor of electromagnetic and radio frequency engineering at the University of Bradford, U.K. He is also the Leader of radio frequency, propagation, sensor design and signal processing; in addition to leading the Communications research group for years with the School of Engineering and Informatics, University of Bradford. He is also a principal investigator for several funded applications to EPSRCs and a Leader of several successful knowledge transfer programmes such as with Arris (previously known as Pace plc), Yorkshire Water plc, Harvard Engineering plc, IETG Ltd, Seven Technologies Group, Emkay Ltd, and Two World Ltd. He has also been a co-investigator in several funded research projects including: 1) H2020 MARIE Skłodowska-CURIE ACTIONS: Innovative Training Networks *Secure Network Coding for Next Generation Mobile Small Cells 5G-US*, 2) Nonlinear and demodulation mechanisms in biological tissue (Department of Health, Mobile Telecommunications & Health Research Programme) and 3) Assessment of the Potential Direct Effects of Cellular Phones on the Nervous System (EU: collaboration with six other major research organizations across Europe). He has published over 500 academic journal and conference papers; in addition he is co-authors of three books and several book chapters. His research interests include computational methods and optimizations, wireless and mobile communications, sensor design, EMC, beam steering antennas, energy efficient PAs, and RF predistorter design applications. He is the fellow of the Institution of Engineering and Technology, a fellow of the Higher Education Academy, and a Chartered Engineer. He received the business Innovation Award for his successful KTP with Pace and Datong companies on the design and implementation of MIMO sensor systems and antenna array design for service localizations. He is the chair of several successful workshops on Energy Efficient and Reconfigurable Transceivers: Approach towards Energy Conservation and CO2 Reduction that addresses the biggest challenges for the future wireless systems. He has also appointed as the Guest Editor for the *IET Science, Measurements and Technology* Journal since 2009 and 2012.

• • •